Substitution of $[Ru_{10}C_2(CO)_{24}]^{2-}$ with Allene. Reversible Formation of $[Ru_{10}C_2(CO)_{22}(\mu\text{-}\eta^2\text{:}\eta^2\text{-}C_3H_4)]^{2-}$ and $[Ru_{10}C_2(CO)_{20}(\mu\text{-}\eta^2\text{:}\eta^2\text{-}C_3H_4)_2]^{2-}$

Kwangyeol Lee and John R. Shapley*

Department of Chemistry, University of Illinois, Urbana, Illinois 61801

Received June 15, 1998

Substitution of carbonyl ligands in $[Ru_{10}C_2(CO)_{24}]^{2-}$ (**1**) by allene (1,2-propadiene) proceeds cleanly in diglyme at 90 °C (1 atm) to afford the monoallene derivative $[Ru_{10}C_2(CO)_{22}(\mu\text{-}\eta^2\text{:}\eta^2\text{-}C_3H_4)]^{2-}$ (**2**). Treatment of either **1** or **2** with allene at 140 °C (1 atm) forms the disubstituted derivative $[Ru_{10}C_2(CO)_{20}(\mu\text{-}\eta^2\text{:}\eta^2\text{-}C_3H_4)_2]^{2-}$ (**3**) in high yield. The new clusters have been isolated as salts with $[PPN]^+$ or $[PPh_3CH_2CH_2PPh_3]^{2+}$ counterions and have been characterized by analytical, spectroscopic, and X-ray crystallographic methods. The framework structures of both molecular cluster anions **2** and **3** are based on edge-shared bioctahedra, with the allene ligands bridging one or two pairs of apical positions, respectively. The idealized symmetries are C_2 for **2** and D_2 for **3**. The solution structures and dynamics of **2** and **3** have been studied by ^{13}C NMR spectroscopy, including variable-temperature and $^{13}C-^{13}C$ COSY experiments.

Introduction

Only a few higher nuclearity cluster systems have been examined for systematic hydrocarbon ligand chemistry, with most known derivatives based on the octahedral $Ru_6(\mu_6\text{-}C)$ framework.[1,2] The decaruthenium cluster $[Ru_{10}C_2(CO)_{24}]^{2-}$ adopts a structure that can be viewed as two Ru_6C octahedra sharing a common edge.[3] This partial fusion of subunits creates a new type of substitution site on the cluster frame, namely, an "inner" site at or near the area of fusion that contrasts with the typical "outer" site on the convex surface of the cluster. We have shown that $[Ru_{10}C_2(CO)_{24}]^{2-}$ undergoes substitution with diphenylacetylene at 125 °C to form $[Ru_{10}C_2(CO)_{22}(\mu\text{-}\eta^2\text{:}\eta^2\text{-}C_2Ph_2)]^{2-}$,[4a] in which the alkyne ligand is in an "inner" position bridging an apical−apical Ru−Ru bond. The substitution is reversed under a carbon monoxide atmosphere at 125 °C, which is a testament to the robust nature of the $Ru_{10}C_2$ framework. In addition, $[Ru_{10}C_2(CO)_{24}]^{2-}$ undergoes oxidative substitution with diphenylacetylene and ferrocenium to form a neutral alkyne derivative $Ru_{10}C_2(CO)_{23}(C_2Ph_2)$, which is then transformed into the reduced complex $[Ru_{10}C_2(CO)_{22}(C_2Ph_2)]^{2-}$ by the action of hydroxide.[4b]

To further explore the reactivity of $[Ru_{10}C_2(CO)_{24}]^{2-}$, we have examined its interaction with allene, which has two orthogonal π bonds and is a potential 4-e ligand. We have found that the reaction of $[Ru_{10}C_2(CO)_{24}]^{2-}$ (**1**) with allene in diglyme at 90 °C provides a monosubstituted derivative $[Ru_{10}C_2(CO)_{22}(\mu\text{-}\eta^2\text{:}\eta^2\text{-}C_3H_4)]^{2-}$ (**2**), which displays substitution at an inner, bridging site. Furthermore, reaction with allene at 140 °C gives a disubstituted derivative, $[Ru_{10}C_2(CO)_{20}(\mu\text{-}\eta^2\text{:}\eta^2\text{-}C_3H_4)_2]^{2-}$ (**3**). Both allene ligands can be removed under CO pressure (see Scheme 1). In this paper, we report the preparations, the solid-state structures, and ^{13}C NMR studies of these allene-substituted $Ru_{10}C_2$ compounds.

Experimental Section

Materials and Methods. All reactions were carried out under a nitrogen atmosphere by using standard inert atmosphere techniques.[5] Diglyme (Aldrich) was dried over molten sodium and distilled immediately before use. The reagents [PPN]Cl (Aldrich), $[Ph_3PC_2H_4PPh_3]Br_2$ (Alfa), allene (PCR), carbon monoxide (MG Industries), and ^{13}CO (99.2%, Isotec) were used as received. The compound $[PPN]_2[Ru_{10}C_2(CO)_{24}]$ was prepared according to the literature.[3a,4a] IR spectra were recorded on a Perkin-Elmer 1750 FT-IR spectrometer. ^1H

(1) (a) Shriver, D. F., Kaesz, H. D., Adams, R. D., Eds. *The Chemistry of Metal Cluster Complexes*; VCH Publishers: New York, 1990. (b) Ma, L.; Williams, G. K.; Shapley, J. R. *Coord. Chem. Rev.* **1993**, *128*, 261. (c) Dyson, P. J.; Johnson, B. F. G.; Martin, C. M. *Coord. Chem. Rev.* **1996**, *155*, 69.

(2) (a) Mallors, R. L.; Blake, A. J.; Parsons, S.; Johnson, B. F. G.; Dyson, P. J.; Braga, D.; Grepioni, F.; Parisini, E. *J. Organomet. Chem.* **1997**, *532*, 133. (b) Blake, A. J.; Haggitt, J. L.; Johnson, B. F. G.; Parsons, S. *J. Chem. Soc., Dalton Trans.* **1997**, 991. (c) Mallors, R. L.; Blake, A. J.; Dyson, P. J.; Johnson, B. F. G.; Parsons, S. *Organometallics* **1997**, *16*, 1668. (d) Brown, D. B.; Dyson, P. J.; Johnson, B. F. G.; Martin, C. M.; Parker, D. G.; Parsons, S. *J. Chem. Soc., Dalton Trans.* **1997**, 1909. (e) Brown, D. B.; Johnson, B. F. G.; Martin, C. M.; Parsons, S. *J. Organomet. Chem.* **1997**, *536*, 285. (f) Johnson, B. F. G.; Matters, J. M.; Gaede, P. E.; Ingham, S. L.; Choi, N.; McPartlin, M.; Pearsall, M. A. *J. Chem. Soc., Dalton Trans.* **1997**, 3251. (g) Johnson, B. F. G.; Shephard, D. S.; Braga, D.; Grepioni, F.; Parsons, S. *J. Chem. Soc., Dalton Trans.* **1997**, 3563. (h) Johnson, B. F. G.; Shephard, D. S.; Braga, D.; Grepioni, F.; Parsons, S. *J. Chem. Soc., Dalton Trans.* **1998**, 311. (i) Braga, D.; Grepioni, F.; Scaccionoce, L.; Johnson, B. F. G. *J. Chem. Soc., Dalton Trans.* **1998**, 1321. (j) Adams, R. D.; Wu, W. *Organometallics* **1993**, *12*, 1238. (k) Adams, R. D.; Wu, W. *Organometallics* **1993**, *12*, 1243. (l) Lee, K.; Hsu, H.-F.; Shapley, J. R. *Organometallics* **1997**, *16*, 3876. (m) Hsu, H.-F.; Wilson, S. R.; Shapley, J. R. *Organometallics* **1997**, *16*, 4937.

(3) (a) Hayward, C.-M. T.; Shapley, J. R.; Churchill, M. R.; Bueno, C.; Rheingold, A. L. *J. Am. Chem. Soc.* **1982**, *104*, 7347. (b) Churchill, M. R.; Bueno, C.; Rheingold, A. L. *J. Organomet. Chem.* **1990**, *395*, 85.

(4) (a) Ma, L.; Rodgers, D. P. S.; Wilson, S. R.; Shapley, J. R. *Inorg. Chem.* **1991**, *30*, 3591. (b) Benson, J. W.; Ishida, T.; Lee, K.; Wilson, S. R.; Shapley, J. R. *Organometallics* **1997**, *16*, 4929.

(5) Shriver, D. F.; Drezdzon, M. A. *The Manipulation of Air-Sensitive Compounds*, 2nd ed.; Wiley: New York, 1986.

S0276-7333(98)00486-5 CCC: $15.00
Publication on Web 08/11/1998

Scheme 1

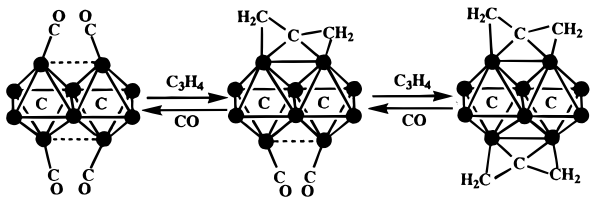

NMR spectra were recorded on General Electric QE 300 (300 MHz) spectrometer. ^{13}C NMR spectra were recorded on General Electric QE 300 (75 MHz), General Electric GN 500 (125 MHz), Varian Unity 400 (100 MHz), and Varian Unity 500 (125 MHz) spectrometers. FAB(−) mass spectra and elemental analyses were obtained by the staffs of the Mass Spectrometry Center and the Microanalytical Laboratory of the School of Chemical Sciences, respectively.

Preparation of $[PPN]_2[Ru_{10}C_2(CO)_{22}(C_3H_4)]$. A diglyme (30 mL) solution of $[PPN]_2[Ru_{10}C_2(CO)_{24}]$ (30.0 mg, 0.0108 mmol) was prepared in a 100 mL three-necked flask equipped with a reflux condenser. Allene was bubbled through the solution for 1 min, and then the solution was heated to 90 °C under the allene atmosphere. The solution color slowly changed from dark purple to bright purple. After 3 h, a completely new set of IR peaks at 2005 (s, sh) and 1998 (vs) cm^{-1} corresponding to $[PPN]_2[Ru_{10}C_2(CO)_{22}(C_3H_4)]$ was observed. Further heating for 0.5 h did not change the IR spectrum. The reaction was stopped, and the solvent was removed under vacuum. The residue was crystallized from dichloromethane/1-propanol (23.4 mg, 0.0084 mmol, 78%). Anal. Calcd for $C_{99}H_{64}O_{22}N_2P_4Ru_{10}$: C, 42.96; H, 2.33; N, 1.01. Found: C, 42.69; H, 2.24; N, 0.90. FAB(−) mass spectrum (^{102}Ru): m/z 1700 ($[Ru_{10}C_2(CO)_{22}(C_3H_4)]^-$) and 1700−28$x$, x = 1−4. IR (CH_2Cl_2): ν_{CO}, 2043(w), 2005(s,sh), 1998(vs), 1958(w,br), 1783(m,br) cm^{-1}. ^1H NMR (CD_2Cl_2, 20 °C): δ 7.67−7.44 (m, 60H), 4.96 (t, 2H, $J + J' = 4.4$ Hz), 4.57 (t, 2H, $J + J' = 4.4$ Hz). ^{13}C NMR (DMF-d_7, 20 °C): δ 246.0 (s, 2C), 245.1 (s, 2C), 207.3 (d, 2C, $J = 5.0$ Hz), 206.6 (d, 2C, $J = 7.1$ Hz), 205.1 (d, 2C, $J = 7.1$ Hz), 204.2 (d, 2H, $J = 6.6$ Hz), 203.8 (d, 2C, $J = 6.6$ Hz), 203.1 (s, 4C), 194.4 (s, 2C), 193.3 (s, 2C).

Preparation of $[PPN]_2[Ru_{10}C_2(CO)_{20}(C_3H_4)_2]$. A. A diglyme (20 mL) solution of $[PPN]_2[Ru_{10}C_2(CO)_{22}(C_3H_4)]$ (10.2 mg, 0.0037 mmol) was prepared in a 100 mL three-necked flask equipped with a reflux condenser. Allene was bubbled through the solution for 1 min, and then the solution was heated to 140 °C under the allene atmosphere. The solution color slowly changed from bright purple to red-purple, and after 2.5 h only the IR peaks corresponding to the product were observed. The reaction flask was cooled, and the solvent was removed under vacuum. The residue was dissolved in dichloromethane, and the solution was layered with 2-propanol. Platelike crystals (8.1 mg, 0.0029 mmol, 80%) were collected following solvent diffusion. Anal. Calcd for $C_{100}H_{68}O_{20}N_2P_4Ru_{10}$: C, 43.64; H, 2.49; N, 1.02. Found: C, 43.55; H, 2.42; N, 1.00. FAB(−) mass spectrum (^{102}Ru): m/z 1684 ($[Ru_{10}C_2(CO)_{22}(C_3H_4)]^-$) and 1656 ($[Ru_{10}C_2(CO)_{21}(C_3H_4]^-$). IR ($CH_2Cl_2$): ν_{CO}, 1996(s,sh), 1993(vs), 1945(m,br), 1915(w,br), 1786(m,br) cm^{-1}. ^1H NMR (CD_2Cl_2, 20 °C): δ 7.68−7.45 (m, 60H), 4.72 (t, 2H, $J + J' = 4.8$ Hz), 4.48 (t, 2H, $J + J' = 4.8$ Hz). ^{13}C NMR (DMF-d_7, 20 °C): δ 248.0 (s, 4C), 205.9 (d, 4C, $J = 6.3$ Hz), 205.8 (d, 4C, $J = 6.3$ Hz), 201.3 (s, 4C), 193.3 (s, 4C).

B. A diglyme (30 mL) solution of $[PPN]_2[Ru_{10}C_2(CO)_{24}]$ (30.0 mg, 0.0108 mmol) was prepared in a 100 mL three-necked flask equipped with a reflux condenser. Allene was bubbled through the solution for 1 min, and then the solution was heated to 140 °C under the allene atmosphere. The solution color slowly changed from dark purple to bright purple and then to red-purple, and after 2.5 h only the IR peaks corresponding to **3** were observed. Workup as before afforded platelike crystals of $[PPN]_2[Ru_{10}C_2(CO)_{20}(C_3H_4)_2]$ (21.7 mg, 0.0079 mmol, 73%).

Reaction of 2 or 3 with CO. A diglyme (20 mL) solution of $[PPN]_2$[**2**] (5.5 mg, 0.0020 mmol) or $[PPN]_2$[**3**] (5.2 mg, 0.0019 mmol) was prepared in a 300 mL pressure bottle. The pressure bottle was pressurized to 20 psig with carbon monoxide, vented, and again pressurized to 20 psig. The pressure bottle was heated in an oil bath to 125 °C for 9 h and then cooled to room temperature before the pressure was released. In each case the IR spectrum of the solution exhibited only a ν_{CO} peak at 2003 cm^{-1} corresponding to **1**. The solvent was removed under vacuum, and the resulting residue was washed with hexane (ca. 5 mL) and then with 2-propanol (ca. 5 mL) to afford dark solid $[PPN]_2$[**1**] (5.1 mg, 0.0018 mmol, 90% from $[PPN]_2$[**2**] or 4.5 mg, 0.0016 mmol, 84% from $[PPN]_2$[**2**]).

^{13}CO Enrichment of $[PPN]_2[Ru_{10}C_2(CO)_{24}]$. A diglyme (30 mL) solution of $[PPN]_2[Ru_{10}C_2(CO)_{24}]$ (287 mg, 0.103 mmol) was prepared in a 300 mL pressure bottle. The pressure bottle was degassed with three freeze−thaw cycles. The evacuated pressure bottle was connected to a ^{13}CO cylinder, pressurized to approximately 1 atm with ^{13}CO (ca. 5-fold excess), and then heated to 120 °C for 6 days. The pressure bottle was allowed to cool to room temperature, and the solvent was removed under vacuum at room temperature. The residue was dissolved in dichloromethane and then layered with 2-propanol. Needle-shaped crystals (215 mg, ca. 0.077 mmol, ca. 75%) were collected following solvent diffusion at room temperature. Analysis of the molecular ion peak in the negative ion FAB mass spectrum suggested a ^{13}CO enrichment of ca. 90%.

X-ray Crystallography. Crystals of the $[PPN]^+$ salts of **2** and **3** were not suitable for X-ray diffraction studies. The corresponding salts of the $[PPh_3CH_2CH_2PPh_3]^{2+}$ counterion were prepared by metathesis in acetone, and the crystals used for the X-ray diffraction studies were grown by slow evaporation from acetone/methanol solutions at room temperature. The data crystal for $[PPh_3CH_2CH_2PPh_3]$[**2**] as the acetone solvate (dimensions 0.05 × 0.08 × 0.44 mm^3) exhibited rather weak diffraction. Both data collections were carried out at 198(2) K on a Siemens SMART/CCD automated diffractometer. All data processing was performed with the integrated program package SHELXTL.[6] Absorption corrections were semiempirical for $[PPh_3CH_2CH_2PPh_3][Ru_{10}C_2(CO)_{22}(C_3H_4)]\cdot 2C_3H_6O$ and analytical by integration for $[PPh_3CH_2CH_2PPh_3][Ru_{10}C_2(CO)_{20}(C_3H_4)_2]\cdot 2C_3H_6O$. Selected crystallographic data are listed in Table 1, and full details are provided in the Supporting Information. The structures were solved by direct methods.[7] Hydrogen atoms were not included in the final structure factor calculations. Only the ruthenium atoms were refined with anisotropic thermal coefficients for the cluster **2**, but all non-hydrogen atoms were refined with anisotropic thermal coefficients for the study involving cluster **3**. Successful convergences of full-matrix least-squares refinement based on F^2 were indicated by the maximum shift/error for the final cycle. The final difference Fourier maps had some high peaks around ruthenium atoms. Metal−metal distances in the cluster cores for both compounds are listed in Table 2, and selected parameters for the allene ligands in complex **3** are collected in Table 3.

Results and Discussion

Synthesis and Characterization of 2 and 3. The reaction of **1** with allene in diglyme proceeds cleanly in two separable stages. At 90 °C with 1 atm allene there

(6) Sheldrick, G. M. *SHELXTL PC, Version 5.0*; Siemens Industrial Automation, Inc.: Madison, WI, 1994.
(7) Sheldrick, G. M. *Acta Crystallogr.* **1990**, *A46*, 467.

Table 1. Crystallographic Data for $[PPh_3CH_2CH_2PPh_3][Ru_{10}C_2(CO)_{22}(C_3H_4)]\cdot 2C_3H_6O$ and $[PPh_3CH_2CH_2PPh_3][Ru_{10}C_2(CO)_{20}(C_3H_4)_2]\cdot 2C_3H_6O$

formula	$C_{71}H_{50}O_{24}P_2Ru_{10}$	$C_{72}H_{54}O_{22}P_2Ru_{10}$
fw	2359.75	2343.79
cryst syst	triclinic	triclinic
space group	$P\bar{1}$	$P\bar{1}$
a (Å)	12.7135(3)	12.7051(4)
b (Å)	15.1959(4)	15.2874(4)
c (Å)	20.2202(6)	20.2833(6)
α (deg)	104.933(1)	105.167(1)
β (deg)	96.895(1)	97.050(1)
γ (deg)	94.367(1)	94.413(1)
V (Å^3)	3723.8(2)	3749.1(2)
Z	2	2
wavelength (Å)	0.710 73	0.710 73
ρ_c (g cm^{-3})	2.105	2.076
μ (mm^{-1})	2.086	2.070
trans coeffs, max/min	0.6517/0.2929	0.8610/0.5695
no. reflns collected	14 375	16 717
no. indep reflns	9602	10 289
R_{int}	0.1091	0.0372
R1 [$I > 2\sigma(I)$][a]	0.1122	0.0470
wR2[b]	0.2803	0.1197

[a] $R1 = \sum|(F_o - F_c)|/\sum|F_o|$. [b] $wR2 = \{\sum[w(F_o^2 - F_c^2)^2]/\sum w(F_o^2)^2]\}^{1/2}$.

Table 2. Ru−Ru Distances (Å) for $[Ru_{10}C_2(CO)_{22}(C_3H_4)]^{2-}$ (2) and $[Ru_{10}C_2(CO)_{20}(C_3H_4)_2]^{2-}$ (3)

	2	3
Apical−Equatorial (CO Bridged)		
Ru1−Ru3	2.802(3)	2.819(1)
Ru2−Ru4	2.812(3)	2.832(1)
Ru5−Ru6	2.815(3)	2.826(1)
Ru7−Ru8	2.812(3)	2.834(1)
Apical−Equatorial (Not Bridged)		
Ru1−Ru2	2.957(3)	2.962(1)
Ru3−Ru4	2.930(3)	2.949(1)
Ru5−Ru7	2.929(3)	2.947(1)
Ru6−Ru8	2.951(3)	2.948(1)
Apical−Hinge		
Ru8−Ru9	2.871(3)	2.908(1)
Ru1−Ru9	3.028(3)	2.990(1)
Ru1−Ru10	2.888(3)	2.937(1)
Ru8−Ru10	3.002(3)	2.958(1)
Ru5−Ru9	2.997(3)	2.979(1)
Ru4−Ru9	2.914(3)	2.940(1)
Ru4−Ru10	2.987(3)	2.954(1)
Ru5−Ru10	2.925(3)	2.944(1)
Hinge−Hinge		
Ru9−Ru10	2.846(3)	2.856(1)
Equatorial−Hinge		
Ru2−Ru9	2.882(3)	2.893(1)
Ru7−Ru9	2.924(3)	2.924(1)
Ru3−Ru10	2.878(3)	2.885(1)
Ru6−Ru10	2.871(3)	2.873(1)
Equatorial−Equatorial		
Ru2−Ru3	2.942(3)	2.954(1)
Ru6−Ru7	2.926(3)	2.934(1)
Apical−Apical		
Ru1−Ru8	3.135(3)	3.084(1)
Ru4−Ru5	3.049(3)	3.038(1)

is complete conversion of **1** to **2** over a period of 3.5 h as signaled by changes in the IR spectrum and a slight change in solution color. The $[PPN]^+$ salt has been isolated from this reaction in 78% yield, and no other product has been indicated. Reaction with allene at 140 °C converts **2** to **3** over a period of 2.5 h with further changes in solution color and IR spectrum. Also, **3** can be formed directly from **1** by reaction with allene at the elevated temperature. The isolated yields of the $[PPN]^+$ salt of **3** are again high (73−80%), and no other product has been observed. It is noteworthy that there is no evidence in these reactions for the variety of products, derived from alternative binding modes as well as coupling reactions, that have typified the interaction of allene with di- and trinuclear iron triad carbonyl compounds.[8]

Table 3. Structural Parameters for the Allene Ligands in $[Ru_{10}C_2(CO)_{20}(C_3H_4)_2]^{2-}$

Distances (Å)			
Ru4−C55	2.10(1)	Ru1−C15	2.13(1)
Ru5−C55	2.11(1)	Ru8−C15	2.17(2)
Ru4−C55B	2.20(1)	Ru1−C15B	2.27(1)
Ru5−C55A	2.23(1)	Ru8−C15A	2.25(1)
C55−C55A	1.39(1)	C15−C15A	1.56(2)
C55−C55B	1.40(1)	C15−C15B	1.43(2)
Angles (deg)			
Ru4−C55−C55A	130.9(7)	Ru1−C15−C15A	128.6(10)
Ru4−C55−C55B	74.6(6)	Ru1−C15−C15B	76.7(9)
Ru4−C55B−C55	67.3(6)	Ru1−C15B−C15	65.6(8)
Ru5−C55−C55A	76.2(6)	Ru8−C15−C15A	72.1(9)
Ru5−C55−C55B	132.3(8)	Ru8−C15−C15B	134.0(10)
Ru5−C55A−C55	66.5(6)	Ru8−C15A−C15	66.7(7)
C55A−C55−C55B	145.2(10)	C15A−C15−C15B	147.3(11)

The formulations of **2** and **3** are clear from their negative ion FAB mass spectra, which show ion multiplets for the cluster molecules as well as ions for formulas corresponding to loss of one or more carbonyl ligands. The presence of the allene ligands, in positions of relatively high symmetry, is also clear from the ^{1}H NMR spectra for **2** and **3**; in each case there are just two pseudotriplets for the allenic protons. The triplets are not of 1:2:1 relative intensities, and homonuclear decoupling experiments have verified that the pattern is due to an AA′XX′ spin system. There is no evidence in the spectrum for exchange between the two proton sites at sample temperatures up to 140 °C. Similar ^{1}H NMR spectra and lack of dynamic behavior characterize the μ-η^2:η^2-C_3H_4 ligand in previously reported dinuclear complexes.[9]

Heating a solution of either **2** or **3** under a modest pressure of carbon monoxide at 125 °C completely displaces the allene ligands to give **1** in high yield. This robust character of the $Ru_{10}C_2$ framework during ligand substitution reactions is summarized in Scheme 1. This stability can also be used to advantage for the direct enrichment of **1** with ^{13}CO at 120 °C.

Solid-State Structures of Clusters 2 and 3. Structural diagrams of the cluster molecules **2** and **3** are shown in Figures 1 and 2, respectively. In both cases the overall geometry of the 10 ruthenium atoms is based on the edge-shared bioctahedral framework of precursor **1**. In **2** the single allene ligand bridges two adjacent

(8) (a) Spetseris, N.; Norton, J. R.; Rithner, C. D. *Organometallics* **1995**, *14*, 603. (b) Ben-Shoshan, R.; Pettit, R. *Chem. Commun.* **1968**, 247. (c) Davis, R. E. *Chem. Commun.* **1968**, 248. (d) Johnson, B. F. G.; Lewis, J.; Raithby, P. R.; Sankey, S. W. *J. Organomet. Chem.* **1982**, *231*, C65. (e) Deeming, A. J.; Arce, A. J.; Sanctis, Y. D.; Bates, P. A.; Hursthouse, M. B. *J. Chem. Soc., Dalton Trans.* **1987**, 2935.

(9) (a) Chisholm, M. H.; Rankel, L. A.; Bailey, W. I., Jr.; Cotton, F. A.; Murillo, C. A. *J. Am. Chem. Soc.* **1977**, *99*, 1261. (b) Lewis, L. N.; Huffmann, J. C.; Caulton, K. G. *J. Am. Chem. Soc.* **1980**, *102*, 403. (c) Hoel, E. L.; Ansell, G. B.; Leta. S. *Organometallics* **1986**, *5*, 585. (d) Kreiter, C. G.; Leyendecker, M.; Sheldrick, W. S. *J. Organomet. Chem.* **1986**, *302*, 35. (e) Kreiter, C. G.; Michels, W.; Heeb, G. Z. *Naturforsch.* **1995**, *50b*, 649. (f) Wu, I. Y.; Tseng, T. W.; Chen, C. T.; Cheng, M. C.; Lin, Y. C.; Wang, Y. *Inorg. Chem.* **1993**, *32*, 1539.

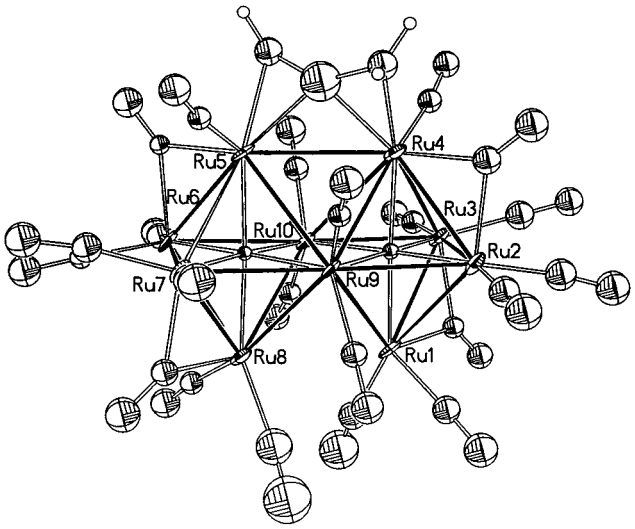

Figure 1. Structural diagram for $[Ru_{10}C_2(CO)_{22}(\mu\text{-}\eta^2\text{:}\eta^2\text{-}C_3H_4)]^{2-}$ (**2**) (35% thermal ellipsoids) showing the metal atom labeling.

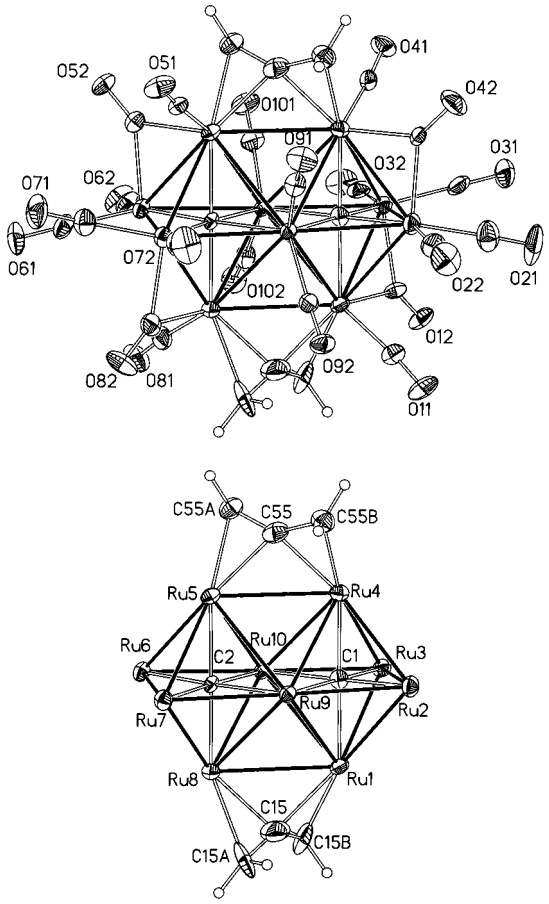

Figure 2. Structural diagrams for $[Ru_{10}C_2(CO)_{20}(\mu\text{-}\eta^2\text{:}\eta^2\text{-}C_3H_4)_2]^{2-}$ (**3**) (35% thermal ellipsoids). Top: entire molecule with carbonyl oxygen atoms labeled. Bottom: $Ru_{10}C_2$ framework and allene ligand labeling.

apical ruthenium atoms, Ru4 and Ru5, exhibiting a $\mu\text{-}\eta^2\text{:}\eta^2$ bonding mode. In **3** both allene ligands adopt this bonding mode, bridging the two pairs of apical ruthenium atoms, Ru4−Ru5 and Ru1−Ru8. In both cases all carbonyls are terminal except for the four bridging carbonyls positioned on the Ru1−Ru3, Ru2−Ru4, Ru5−Ru6, and Ru7−Ru8 edges. An analogous distribution of bridging carbonyls was seen in the structures of both **1**[3] and $[Ru_{10}C_2(CO)_{22}(C_2Ph_2)]^{2-}$.[4a] For **2** these ligand distributions result in an idealized molecular symmetry of C_2, with the C_2 axis passing through the central allene carbon and bisecting the hinge Ru−Ru bond. For **3** the idealized symmetry becomes D_2, which is the same as for precursor **1**.

Table 4. Comparison of Average Ru−Ru Distances (Å) for 1, 2, and 3

	1	2	3
	Apical−Equatorial (CO Bridged)		
	2.813	2.810	2.828
	Apical−Equatorial (Not Bridged)		
	2.983	2.942	2.951
	Apical−Hinge		
short	2.863	2.900	2.932
long	3.088	3.004	2.970
all	2.976	2.952	2.951
	Hinge−Hinge		
	2.872	2.846	2.856
	Equatorial−Hinge		
	2.902	2.889	2.894
	Equatorial−Equatorial		
	2.940	2.934	2.944
	Apical−Apical		
	3.130	3.092	3.061

The limited precision achieved in the structural study of **2** precludes quantitative discussion of the light atom positions, but the higher quality data obtained for **3** allow evaluation of the structural parameters for the allene ligands, which are listed in Table 3. The allene ligand bridging the Ru4−Ru5 vector is well ordered and symmetrical, with Ru−C distances to the central carbon (Ru4−C55 = 2.10(1) and Ru5−C55 = 2.11(1) Å) that are ca. 0.1 Å longer than the Ru−C distances to the terminal carbons (Ru4−C55B = 2.20(1) and Ru5−C55A = 2.23(1) Å). This feature and the C−C distances (C55−C55A = 1.39(1) and C55−C55B = 1.40(1) Å) and the C−C−C angle (C55A−C55−C55B = 145(1)°) are entirely typical of structurally characterized allene ligands with this bonding mode.[9] The parameters for the allene ligand bridging Ru1 and Ru8 are somewhat less well-defined, but the general structural features for this ligand are the same as for the other $\mu\text{-}\eta^2\text{:}\eta^2$ cases.

Metal−metal distances determined for the Ru_{10} frameworks in **2** and **3** are summarized in Table 2. Average Ru−Ru distances in various categories are compared for **2** and **3** as well as **1** in Table 4. The overall distributions of the Ru−Ru distances in **1**, **2**, and **3** are very similar. In all cases the CO-bridged apical−equatorial Ru−Ru distances are the shortest and the apical−apical Ru−Ru distances are the longest, with a range of ca. 0.3 Å. The edge shared by the two carbide-centered octahedral subunits, the "inner" hinge−hinge distance, is uniformly among the shorter distances, and the corresponding "outer" equatorial−equatorial distance is 0.07−0.09 Å longer. The apical−hinge distances of the inner region divide into two alternating sets, short and long, with the average difference between the two sets diminishing from **1** (Δ_{av} = 0.23 Å) to **2** (Δ_{av} = 0.10 Å) to **3** (Δ_{av} = 0.04 Å). The degree to which successive allene substitution regularizes this inner region of the metal framework can be appreciated by the comparison of specific distances shown in Figure 3. It is noteworthy that the overall average of all apical−hinge distances is closely

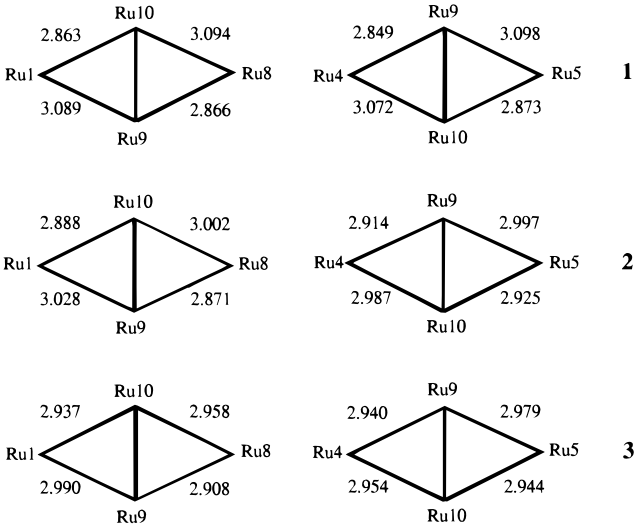

Figure 3. Comparison of the apical−hinge Ru−Ru distances (Å) for $[Ru_{10}C_2(CO)_{24}]^{2-}$ (**1**), $[Ru_{10}C_2(CO)_{22}(C_3H_4)]^{2-}$ (**2**), and $[Ru_{10}C_2(CO)_{20}(C_3H_4)_2]^{2-}$ (**3**).

similar for **1**, **2**, and **3**; however, the average apical−apical distances undergo a steady decrease from 3.130 Å for **1** to 3.092 Å for **2** to 3.061 Å for **3**.

According to the "condensation principle" of polyhedral skeletal electron pair theory,[10] a 10 atom D_{2h} framework formed by fusing two octahedra at a common edge should possess a total of 86 + 86−34 = 138 valence electrons. This calculation presumes no net bonding interaction between the adjacent apical positions of the octahedra. However, a regular structure constructed in this way brings the pairs of apical centers as close together as any of the other edges of the octahedral subunits, and the substantial overlap of metal orbitals results in both bonding and antibonding interactions that sum *formally* to zero apical−apical bond order. Compound **1** was the first example of the edge-fused bioctahedral structure to be characterized,[3] and its valence electron count of 138 helped to provoke development of the condensation principle.[10b] However, the structure of **1** shows two distortions in the metal framework in response to the nonbonded interactions between the apical metal centers, viz., the apical−apical Ru−Ru distances elongate (>3.1 Å), to become by a slight margin the longest in the molecule, and the two subunits twist about their point of fusion, which reduces the overall symmetry to D_2 and generates the strong alternation in the apical−hinge Ru−Ru distances shown in Figure 3.

Compounds **2** and **3** also have 138 valence electrons and display the same basic bioctahedral structure as **1**. However, in **2** and **3**, the presence of a hydrocarbon ligand capable of bridging two adjacent apical sites changes the balance of bonding versus antibonding interactions between these sites. Some of the combinations of metal-based orbitals that are antibonding between the metal centers are just those that are suitable for π-back-bonding to the bridging ligand. Thus, in forming the complex with allene, these metal−metal antibonding orbitals will tend to be stabilized by

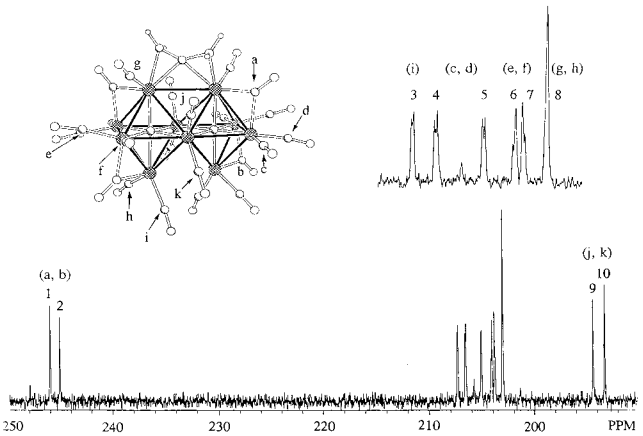

Figure 4. ^{13}C NMR spectrum of ^{13}CO-enriched $[Ru_{10}C_2(CO)_{22}(C_3H_4)]^{2-}$ (**2**) showing the assignments.

mixing with metal−ligand bonding orbitals, resulting in a net increase in apical Ru−Ru bonding and a concomitant shortening of the apical−apical Ru−Ru distances. These effects are relatively modest for the bridging allene ligand; the bridged distance in **2** (3.049(3) Å) is only 0.09 Å shorter than the unbridged distance (3.135(3) Å), and the presence of two allene bridges in **3** results in apical−apical distances averaging only 0.07 Å shorter than those in **1**. The effects of substitution are much more dramatic in the alkyne complex $[Ru_{10}C_2(CO)_{22}(\mu\text{-}\eta^2\text{:}\eta^2\text{-}C_2Ph_2)]^{2-}$,[4a] which displays a severely shortened bridged Ru−Ru distance (2.711(1) Å) and a correspondingly lengthened distance (3.823(1) Å) for the other apical−apical vector. This severe distortion may be the reason we have not been able to observe the disubstituted diphenylacetylene analogue of **3**. In work described elsewhere, however, we have shown that the neutral alkyne complex $Ru_{10}C_2(CO)_{23}(C_2Ph_2)$[4b] reacts with additional alkyne to form a disubstituted derivative; however, in this case the second alkyne bridges unsymmetrically, leading to apical−apical distances of 2.859(1) and 3.139(1) Å.[11]

It should be noted that "counting" metal−metal bonds in **1** and its derivatives is problematical, since many of the Ru−Ru distances that are displayed are significantly longer than the typical Ru−Ru single-bond distance of 2.855(1) Å seen in $Ru_3(CO)_{12}$.[12] The presence of the carbide ligands is undoubtedly the most important factor overall in stabilizing the cluster framework, and the radial Ru−C bonding is probably as strong as or stronger than the peripheral Ru−Ru bonding.[10a] Thus, the Ru−Ru bonding network will tend to undergo distortion, with resulting long or short distances, in response to the optimal electronic or steric requirements of ligands substituting on the periphery. Nevertheless, the overall cluster valence electron count of 138 electrons is maintained in all these cases.

^{13}C NMR Study of 2. The ^{13}C NMR spectrum of ca. 90% ^{13}CO-enriched **2** at room temperature exhibits 10 signals, as shown in Figure 4. Peak 8 of intensity 4C is actually composed of two overlapping 2C signals (vide infra), so the solution spectrum is consistent with the solid-state structure, which has 11 inequivalent pairs

(10) (a) Mingos, D. M. P.; Wales, D. J. *Introduction to Cluster Chemistry*; Prentice Hall: Engelwood Cliffs, NJ, 1990. (b) Mingos, D. M. P. *J. Chem. Soc., Chem. Commun.* **1983**, 706.

(11) (a) Lee, K.; Shapley, J. R. *Organometallics*, submitted for publication. (b) Lee, K. Ph.D. Thesis, University of Illinois, 1997.

(12) Churchill, M. R.; Hollander, F. J.; Hutchison, J. P. *Inorg. Chem.* **1977**, *16*, 2655.

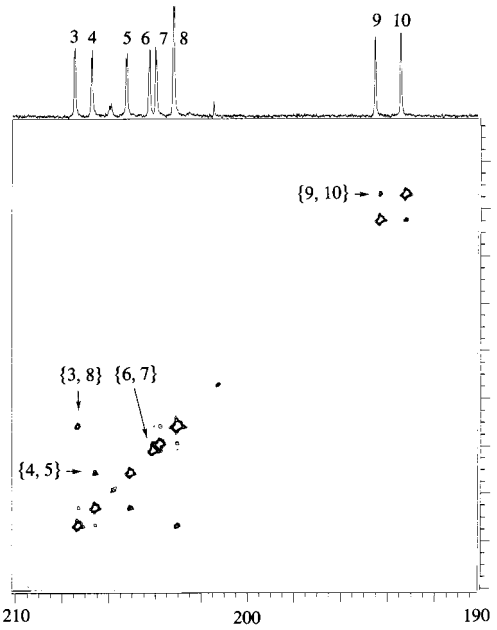

Figure 5. The terminal carbonyl region in the $^{13}C-^{13}C$ COSY spectrum of $[Ru_{10}C_2(CO)_{22}(C_3H_4)]^{2-}$ (**2**).

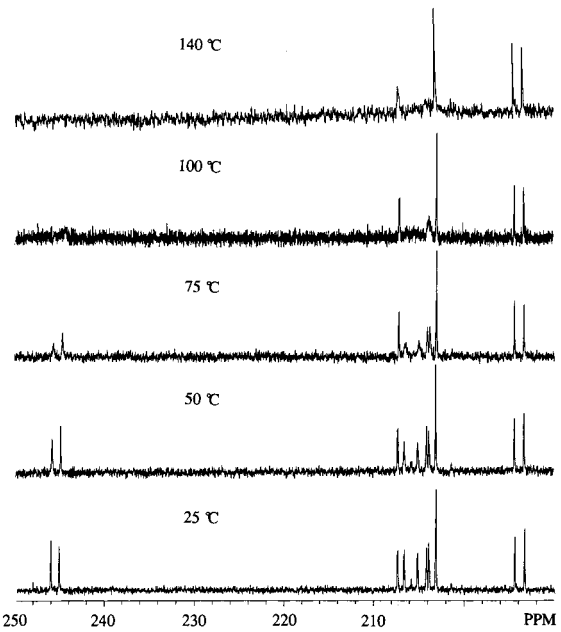

Figure 6. Variable-temperature ^{13}C NMR spectra of $[Ru_{10}C_2(CO)_{22}(C_3H_4)]^{2-}$ (**2**).

of carbonyls under C_2 symmetry. The assignments of the NMR signals to the individual carbonyl positions are also shown in Figure 4. These assignments are based on the following considerations.

(1) Peaks 1 and 2, the most downfield set near δ 245, are assigned to the bridging carbonyls **a** and **b**, whereas peaks 9 and 10, the most upfield set near δ 195, are due to the hinge carbonyls **j** and **k**. Both of these positions and assignments compare closely with those determined previously for compound **1**[3a] and for $[Ru_{10}C_2(CO)_{22}(C_2Ph_2)]^{2-}$ [4a] as well as for **3** discussed below.

(2) At the high level of ^{13}CO enrichment for this sample of **2**, peaks 3−7 show evidence for $^{13}C-^{13}C$ coupling. Peaks 6 and 7 clearly form an AB quartet, indicating the mutual coupling of these sites (J = 6.6 Hz). Peaks 4 and 5 are doublets with a coupling constant of 7.1 Hz. The assigment of these pairs of peaks to the carbonyl pairs (**e**, **f**) and (**c**, **d**), respectively, is based on (i) the asssumption that strong C−C coupling implies that the corresponding carbonyls are geminal, that is, bound to the same ruthenium atom, as well as (ii) the variable-temperature behavior that selectively links these signals with those of the bridging carbonyls (vide infra). Peak 3 is also a doublet, with a splitting of 5.0 Hz, but no obvious coupling partner is seen. The position of this partner as underlying peak 8 has been revealed by the $^{13}C-^{13}C$ COSY spectrum shown in Figure 5.

(3) The COSY spectrum shows four strong correlations, namely {3, 8}, {4, 5}, {6, 7}, and {9, 10}, which is consistent with the four sets of geminal terminal carbonyls, (**h**, **i**), (**c**, **d**), (**e**, **f**), and (**j**, **k**), respectively. Note the obvious correlation between the hinge carbonyls **j** and **k**, even though the coupling constant is not large enough to cause observable splitting in the one-dimensional spectrum (Figure 4). The strong correlation {3, 8} is consistent with the splitting partner of peak 3 being part of peak 8, but these peaks also show correlations with other peaks, namely, {3, 4} and {7, 8}. Furthermore, with more sensitive settings, the additional correlations {1, 8}, {2, 8}, {8, 9}, and {8, 10} can be observed (see figure in Supporting Information). Since the signals for *both* bridging carbonyls **a** and **b** and *both* hinge carbonyls **j** and **k** show correlations similar to peak 8, the two types of carbonyls giving rise to peak 8 must have a consistent geometric relationship with both the bridging carbonyls and the hinge carbonyls. These requirements are met by the sets of carbonyls **g** and **h**, which occupy analogous positions "top" and "bottom" in the structure. Carbonyl **g** is nearly perpendicular to the plane defined by bridging carbonyl **a**, and it forms a small dihedral angle with hinge carbonyl **j**. Carbonyl **h** has similar relationships with bridging carbonyl **b** and hinge carbonyl **k**. Peak 3 then corresponds uniquely with carbonyl position **i** at the "bottom" of the structure; the analogous position adjacent to **g** at the "top" is occupied by the coordinated double bond of the allene ligand.

(4) An NOE experiment irradiating the protons in the allene ligand has been carried out in an attempt to make the assignment more complete. The difference spectrum shows a notable NOE effect on peak 8 and a small effect on peak 1. Thus, the assignment of peak 8 to carbonyls **g** is further supported, since the terminal carbonyls **g** are in closest proximity to the allene ligand. Also, peak 1 is assigned to the bridging carbonyls **a**, which are closer to the allene ligand than bridging carbonyls **b**. Differentiation among hinge carbonyls **j** and **k** is not possible.

(5) Variable-temperature ^{13}C NMR study of **2** has revealed a carbonyl scrambling process. As the temperature is raised, ^{13}C peaks 1, 4, and 5 broaden first at the same rate ($\Delta G^{\ddagger}$ = 19.3 kcal/mol), and at higher temperatures, peaks 2, 6, and 7 broaden at the same rate ($\Delta G^{\ddagger}$ = 20.8 kcal/mol), as shown in Figure 6. Each of these processes is assigned to the localized 3-fold rotation of a set of three carbonyls, with each set composed of one bridging carbonyl and two terminal carbonyls attached to an equatorial ruthenium atom. As labeled in Figure 4, these sets are (**a**, **c**, **d**) and (**b**, **e**,

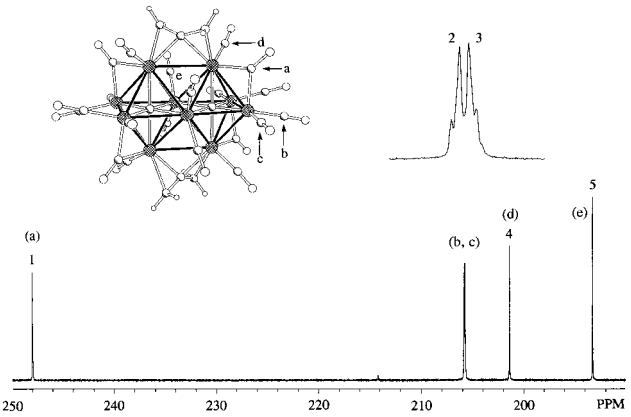

Figure 7. ^{13}C NMR spectrum of ^{13}CO-enriched $[Ru_{10}C_2(CO)_{20}(C_3H_4)_2]^{2-}$ (**3**) showing the assignments.

f). The exchange of bonding modes between a bridging carbonyl and a terminal carbonyl on an apical ruthenium atom, which is present in $[Ru_{10}C_2(CO)_{22}(C_2Ph_2)]^{2-}$, is not observed.[4a] This fluxional process would also require a simultaneous sweeping motion of the allene ligand that would generate an effective mirror plane containing all apical rutheniums. This sweeping motion of the allene ligand is clearly unfavorable for **2**, as evidenced by its ^{1}H NMR spectra.

^{13}C NMR Study of 3. The ^{13}C NMR spectrum of **3** at room temperature (125 MHz) exhibits five signals with 4:4:4:4:4 relative intensities, consistent with the high symmetry expected from the solid-state structure. The spectrum and assignments are shown in Figure 7. Peak 1 in the downfield region is assigned to the bridging carbonyls **a**. Peaks 2 and 3 are doublets of an AB spin system. The coupling constant of 6.3 Hz is similar to those observed in compound **2**. The strong coupling between the signals and the intermediate chemical shift position lead to the assignment of peaks 2 and 3 to the two sets of terminal carbonyls, **b** and **c**, on the equatorial rutheniums. Peak 4 is assigned to the terminal carbonyls **d** on the apical rutheniums, and the most upfield peak 5 is assigned to the carbonyls on the hinge carbonyls **e**. At elevated temperatures, peaks 1, 2, and 3 broaden ($\Delta G^{\ddagger} = 17.5$ kcal/mol) at the same rate, and peaks 4 and 5 do not broaden at all (Figure 8). The dynamic effects are again assigned to 3-fold exchange among the set of one bridging carbonyl and two terminal carbonyls attached to each of the equatorial ruthenium atoms (**a**, **b**, **c**).

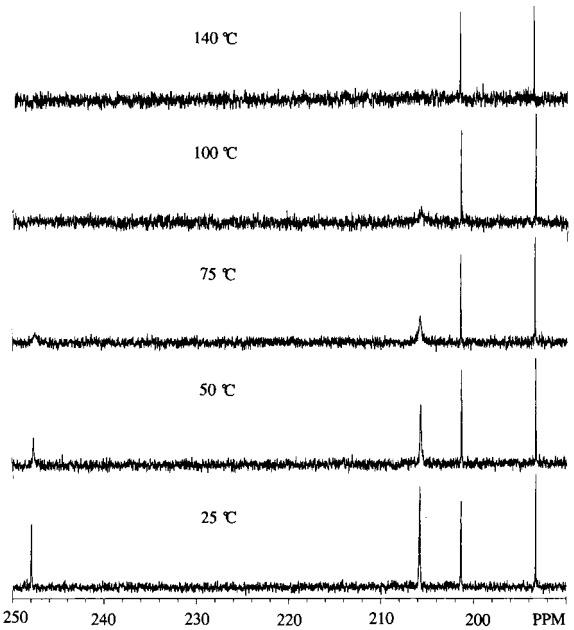

Figure 8. Variable-temperature ^{13}C NMR spectra of $[Ru_{10}C_2(CO)_{20}(C_3H_4)_2]^{2-}$ (**3**).

Acknowledgment. This research was supported by a grant from the National Science Foundation, CHE 9414217 (to J.R.S.). We thank Dr. Scott R. Wilson for X-ray data collection. Purchase of the Siemens Platform/CCD diffractometer by the School of Chemical Sciences at the University of Illinois was supported by National Science Foundation Grant CHE 9503145. NMR spectra were obtained using instruments in the Varian Oxford Instrument Center for Excellence in NMR Laboratory in the School of Chemical Sciences; external funding for this instrumentation was obtained from the Keck Foundation, NIH, and NSF. We particularly thank VOICE NMR Lab Director Dr. Vera Mainz for assistance in conducting the ^{13}C−^{13}C COSY experiment.

Supporting Information Available: Tables of positional parameters, anisotropic thermal parameters, bond distances, and bond angles for the X-ray crystallographic studies of compounds **2** and **3** and a complete ^{13}C−^{13}C COSY spectrum of **2** (33 pages). See any current masthead page for ordering and Internet access instructions.

OM980486G